Available online at www.sciencedirect.com
SCIENCE DIRECT
Polymer 47 (2006) 6131–6139
polymer
www.elsevier.com/locate/polymer

Spectroscopic characterization of polyaniline formed in the presence of montmorillonite clay

Gustavo M. do Nascimento [a,*], Vera R.L. Constantino [a], Richard Landers [b,c], Marcia L.A. Temperini [a,*]

[a] Departamento de Química Fundamental, Instituto de Química, Universidade de São Paulo, CP 26077, CEP 05513-970, São Paulo, SP, Brazil
[b] Departamento de Física Aplicada, Instituto de Física Gleb Wataghin, Universidade Estadual de Campinas, CP 6165, CEP 13083-970, Campinas, SP, Brazil
[c] Laboratório Nacional de Luz Síncrotron, CP 6192, CEP 13084-971, Campinas, SP, Brazil

Received 1 December 2005; received in revised form 9 June 2006; accepted 10 June 2006
Available online 10 July 2006

Abstract

This work shows the spectroscopic characterization of polyaniline–montmorillonite clay (PANI–MMT) composites prepared by polymerization of aniline in aqueous suspensions of montmorillonite clay and camphorsulfonic acid containing persulfate ions as oxidizing agent. X-ray diffraction, scanning electron microscopy, and X-ray absorption near Silicon *K*-edge data show that morphologies and structures of PANI–MMT nanocomposites depend on their relative amount. The electrical conductivity values of composites increase from 10^{-4} to 10^{-1} S/cm^{-1} when PANI–MMT ratio increases, and percolation threshold is observed when polymer/clay mass ratio is changed. Resonance Raman, UV–VIS–NIR spectroscopy, electron spin resonance (EPR) and X-ray absorption near Nitrogen *K*-edge data confirm that PANI has emeraldine salt form for all PANI–MMT materials prepared.

Keywords: Resonance Raman; Polyaniline; Composites

1. Introduction

The control and enhancement of poly(aniline) (PANI) bulk properties is one of the greatest challenges in conducting polymer area [1]. Synthesis of micro and nanostructured PANI can improve its electrical, thermal and mechanical stabilities [2]. There are many routes for preparing these materials, through micellar media [3], interfacial [4], template-guided [5] or aniline polymerization in presence of inorganic or organic matrices resulting in PANI composites [2,6–8].

Among these synthetic approaches, the formation of PANI nanocomposites has received great attention, once it is possible to use this method to get PANI with ordered chain structure and with better properties than for bulk ones [2,6–8]. The most common inorganic matrix used to prepare PANI composites is smectite montmorillonite clay (MMT) [6–8], due to its capacity to swell and exchange cations. A special type of nanocomposite can be obtained when anilinium (An^+) polymerization is done mainly between the interlayer regions, using anilinium intercalated clay (An^+–MMT) as precursor (this route was used in our previous works [8a,8b]). In another route, aniline polymerization is done in an acidic aqueous suspension of clay (usually Na^+–MMT as precursor) having one oxidizing agent and, in this case, the polymerization does not necessarily occur inside the interlayer region (this route will be used in the present work). Layered silicates like MMT clay have layer thickness of about 10 Å. These negative charged layers are stacked face to face forming crystallites known as tactoids. Structurally, two kinds of clay–polymer nanocomposites can be isolated: (i) *intercalated nanocomposites* where polymer chains are between the tactoids layers and a regular repeating distance can be observed by using X-ray

* Corresponding author. Tel.: +55 11 3091 3853; fax: +55 11 3091 3890.
E-mail address: morari@yahoo.com (G.M. do Nascimento).

0032-3861/$ - see front matter © 2006 Elsevier Ltd. All rights reserved.
doi:10.1016/j.polymer.2006.06.036

diffractometry and/or transmission electron microscopy; (ii) *exfoliated nanocomposite* where clay crystallites are delaminated forming individual layers dispersed within the polymer. When aniline polymerization is done in an acidic aqueous suspension of MMT having one oxidizing agent, the formation of intercalated and/or exfoliated nanocomposite can be dependent on monomer/clay ratio.

Conductivity is one of the desired properties of PANI that must be enhanced when composites are formed. Electrical conductivity of this material is generally characterized by its dependence on the amount of conductive polymeric material. At low PANI loadings, conductivity of composite is still very close to that of insulate pure MMT clay. At some critical loading, called percolation threshold [9], conductivity increases several magnitude orders with a very little increase in the PANI amount. At percolation threshold, continuous conductive network through composite begins to form. After this region of drastic enhancement, conductivity once again levels off and its value is close to that of free PANI.

Nevertheless, nanocomposites of PANI–MMT [6,8] obtained by An^+–MMT polymerization show lower conductivity than free PANI [7]. One reason could be the lack of connectivity between intercalated PANI chains [6,8] or a change in the nature of these polymeric chains. It was demonstrated [8], by using resonance Raman, X-ray absorption near Nitrogen *K*-edge (N *K* XANES) and UV–VIS–NIR spectroscopies, that PANI obtained by aniline polymerization between MMT layers has chains with benzidine (1,4-diamine biphenyl), phenazine-like rings and N=N segments together with ideal conducting sequence of 1,4-phenylenediamine radical cations, dications and neutral repeat units. Using X-ray photoelectron spectroscopy (XPS), it was also possible to verify that on the external surface and edge of clay crystals, polymeric PANI chains were in emeraldine salt form, while Nitrogen *K*-edge XANES data, which come from bulk region of PANI–MMT particles, confirmed the presence of phenazine, azo and amine types of nitrogen in intercalated PANI chains [8].

In a previous work, for PANI–MMT hybrid material prepared by aniline polymerization in an acidic aqueous suspension of Na^+–MMT having one oxidizing agent [8], it was observed that PANI chains are similar to free PANI, having only radical cation, dication, and reduced moieties of 1,4-phenylenediamine repeat units. Nevertheless, these data were for only one PANI–MMT ratio. It has not been characterized by polymeric chain as a function of MMT–PANI ratio in order to know if after and before percolation threshold there is a change in nature of PANI chains.

In this work a spectroscopic characterization of four different PANI–MMT composites prepared by aniline polymerization in an acidic aqueous suspension of Na^+–MMT was done, using resonance Raman, FTIR, Nitrogen *K*-edge XANES, XPS and electron spin resonance (EPR) spectroscopies. Composite morphologies were characterized by scanning electron microscopy (SEM) and their structures by X-ray diffractometry (XRD) and Silicon *K*-edge XANES spectroscopy. Some data were compared to those reported previously [8b] for intercalated nanocomposite PANI–MMT prepared by An^+–MMT polymerization.

2. Experimental section

2.1. Preparation of PANI–MMT composites

Swy2 Montmorillonite (MMT, from Clay Minerals Repository) was treated with sodium chloride and size fractioned to obtain homoionic Na^+-form free of main impurities. An aqueous suspension containing 0.01 g of Na^+–MMT in 100 mL (0.01%) was prepared and sonicated in ultrasonic bath for 1 h to promote interlayer swelling and clay exfoliation/delamination. This Na^+–MMT suspension (75 mL) and 25 mL of a solution containing 1 mol/L camphorsulfonic acid, (−)HCSA (Merck), and 0.5 mol/L of aniline were mixed under stirring at room temperature, and then 2.85 g of ammonium persulfate was slowly added to the suspension. Reaction mixture was maintained under stirring for 10 h. Green solid was isolated by filtration (no washing of the composite was done after the isolation) and dried in desiccator. The general procedure reported above was described in Ref. [7].

The experimental procedure described above was used in the preparation of other PANI–MMT composites with different clay amounts (see Table 1) taking initial 0.1%, 1% and 2.6% Na^+–MMT suspensions. Table 1 shows the expected amount of PANI (wt.% of PANI) in the composites considering the initial mass of all reagents and supposing that all aniline was polymerized. Also Table 1 presents elemental analysis (C,H,N,S) of all materials. The solid samples are here abbreviated as PANI–MMT-*X* where *X* is 1–4, according to Table 1. For comparison purposes, a sample was prepared containing the reagent amounts mentioned above but without the clay addition (hereafter abbreviated PANI–MMT-0).

2.2. Preparation of PANI–MMT composite by An^+–MMT polymerization

The experimental procedure was described in Ref. [8b]. The important step of this procedure is the elimination of non-intercalated anilinium ions from An^+–MMT through exhaustive washing of the material with deionized water. Polymerization medium was an aqueous suspension of An^+–MMT at pH 2 (adjusted with HCl) and ammonium persulfate. After stirring for 12 h at room temperature, a dark green solid was isolated by filtration (no washing of the composites was done after the isolation) and dried in desiccator. The obtained CHN microanalysis of PANI–MMT shows that for An^+–MMT there

Table 1
Expected amount of PANI (wt.% of PANI) in the composites and the elemental analysis (C,H,N,S) of PANI–MMT composites

PANI–MMT composites	Nominal clay (wt./g)	Nominal total (wt./g)[a]	Nominal clay (wt.%)	Nominal PANI (wt.%)	Actual elemental (wt.%) (C + H + N + S)
1	1.95	11.8	16.6	9.9	53.0
2	0.75	10.6	7.10	11	60.0
3	0.075	9.90	0.75	11.8	65.2
4	0.0075	9.83	0.076	11.8	72.2

[a] Aniline + HCSA + clay + ammonium persulfate.

is 3.5 g aniline/100 g of composite, for PANI–MMT prepared at pH 2 there is 2.0 g of polymer/100 g of composite.

2.3. Preparation of PANI-ES and PANI-EB

PANI-ES was prepared using aniline and ammonium persulfate in HCl media, according to procedure described by MacDiarmid et al. [10]. PANI-EB form was prepared through the deprotonation of PANI-ES (according to procedure described by MacDiarmid et al. [10]).

2.4. Instrumentation

Resonance Raman spectra using 632.8 nm and 457.9 nm laser lines as exciting radiation (from He–Ne laser, Spectra Physics, mod 127) were recorded in Renishaw Raman Imaging Microscope (system 3000) containing Olympus metallurgical microscope and CCD detector. The laser beam was focused on sample in ca. 1 μm spot by 80× lens. Laser power was always kept below 0.7 mW at sample in order to avoid its degradation.

EPR spectra of solid samples were recorded at room temperature on Bruker ER 200 spectrometer operating in X-band (~9.5 GHz).

UV–VIS–NIR spectra were obtained in Shimadzu UVPC-3101 scanning spectrophotometer in transmission mode.

XRD patterns of powdered samples were obtained on a Rigaku diffractometer model Miniflex using Cu Kα radiation (1.541 Å, 30 kV, 15 mA, step of 0.05°).

XPS measurements were done using characteristic Kα radiation from Al anode to excite samples and a 100 mm mean radius hemispherical analyzer operated with a constant pass energy of 44 eV, that resulted in 1.6 eV FWHM for Au 4f line. A small quantity of each sample was pressed between two stainless steel plates to form a thin conglomerate that was fixed to sample holder with double faced conducting tape. Analyses were done at a base pressure of 5×10^{-9} mbar and charging effects were corrected by shifting spectra so that C 1s line was at 284.6 eV.

Nitrogen *K*-edge and Silicon *K*-edge XANES spectra were obtained using the facilities of the National Synchrotron Light Laboratory (LNLS), Campinas, Brazil. For collecting Nitrogen *K*-edge XANES spectra, a spherical grating monochromator (SGM) beam line (the spectral resolution $E/\Delta E$ of spherical grating is better than 3000) with focused beam of ca. 0.5 mm^2 spot were used. The spectra were recorded in total electron yield detection and with sample's chamber at ca. 10^{-8} mbar. Measurements were done with sample surface perpendicular to beam. All energy values in Nitrogen *K*-edge spectra were calibrated using the first resonant peak in the Nitrogen *K*-edge XANES spectra for potassium nitrate [11]. The collecting of XANES in Silicon *K*-edge spectra was done using a double Si crystal monochromator with toroidal focusing mirror with focused beam of 2.0×3.0 mm^2 (the spectral resolution $E/\Delta E$ of SXS beam line is better than 5000). Spectra were recorded in total electron yield detection and with sample chamber at ca. 10^{-8} mbar. Measurements were done with sample surface perpendicular to beam. All energy values in Silicon *K*-edge spectra were calibrated using first resonant peak in Silicon *K*-edge XANES spectra for Silicon crystal foil [12].

SEM images of solid samples, recovered by 16 nm of sputtered gold film, were recorded through low vacuum scanning electron microscope (SEM, JSM-5900LV) and operated with a high-tension voltage of 10 kV.

Material resistivities were measured by the two points method using an Autolab PGSTAT30 impedance analyzer (Ecochemie) with FRA module. A d.c. potential of 0.0 V with a modulation of 5 mV (rms) was imposed in the 10 KHz–10 MHz frequency range.

3. Results and discussion

Fig. 1 shows the SEM images of Na^+–MMT, nanocomposite PANI–MMT prepared from intercalated anilinium clay (An^+–MMT), PANI–MMT composites having different monomer/MMT ratio and PANI polymer in emeraldine salt form (PANI-ES). Na^+–MMT (image A) shows primary particles in the micrometer range that consist of face-to-face stacking crystallites (tactoids). The morphology of PANI–MMT composite material with major clay content (image 1) is equal to that of sodium clay (image A), which is similar to the morphology presented by PANI–MMT nanocomposite obtained from An^+–MMT (image B). The three images are distinct from that of free PANI-ES (image C). As the clay content decreases in PANI–MMT materials, morphologies of composites gradually change from clay-type, where tactoids plates domain the image (image 1), to morphologies with the presence of domains where tactoids plates and granular regions like PANI can be seen (images 2 and 3). Finally, when the polymer reaches the highest amount in the composite, the morphology (image 4) is similar to that of free PANI-ES (isolated granules).

Fig. 2 shows the change in the X-ray diffraction patterns of PANI–MMT composites prepared from different monomer/MMT ratio, as described in Section 2. In XRD patterns of PANI–MMT materials with high clay amount (Fig. 2(1–3)), many sharp diffraction peaks of crystalline phases are observed. Some diffraction peaks could be assigned to ammonium persulfate ($d \sim 4.20$ Å/21.1°; $d \sim 3.98$ Å/22.3°) [13a] and ammonium hydrogen sulfate ($d \sim 5.39$ Å/16.4°; $d \sim 4.93$ Å/18.0°, $d \sim 4.66$ Å/19.1°) [13b]. The other narrow diffraction peaks cannot be attributed to MMT, PANI or a salt from the combination of ammonium, sodium, persulfate or sulfate ions. As it can be seen in Table 2, diffraction peak values observed for composite materials can be assigned to HCSA. However, peak intensities of PANI–MMT materials are distinct to those recorded for HCSA (Fig. 2). Probably, the environment affects the HCSA planes growing and, consequently, the peak's intensity. Considering that aniline, HCSA and ammonium persulfate nominal amounts are the same in all materials, it is possible to conclude that MMT clay is responsible for the reagent's crystallization in the composites. Silanol and aluminol groups (≡Si–OH and ≡Al–OH) at clay edges can be interacting,

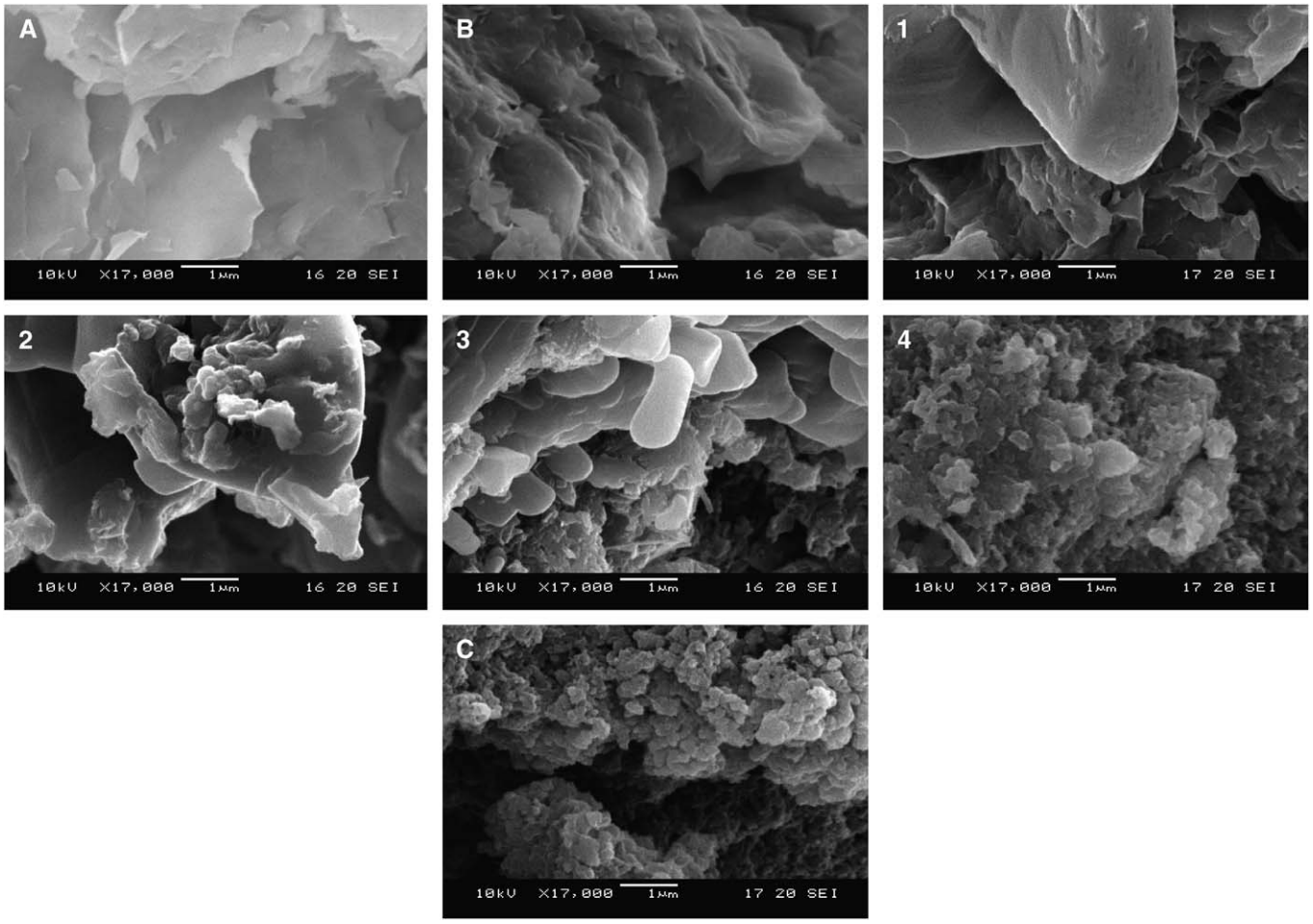

Fig. 1. SEM images of: Na^+–MMT (A); PANI–MMT (from An^+–MMT polymerization) (B); PANI–MMT composites: 1, 2, 3, 4; and PANI-ES (C).

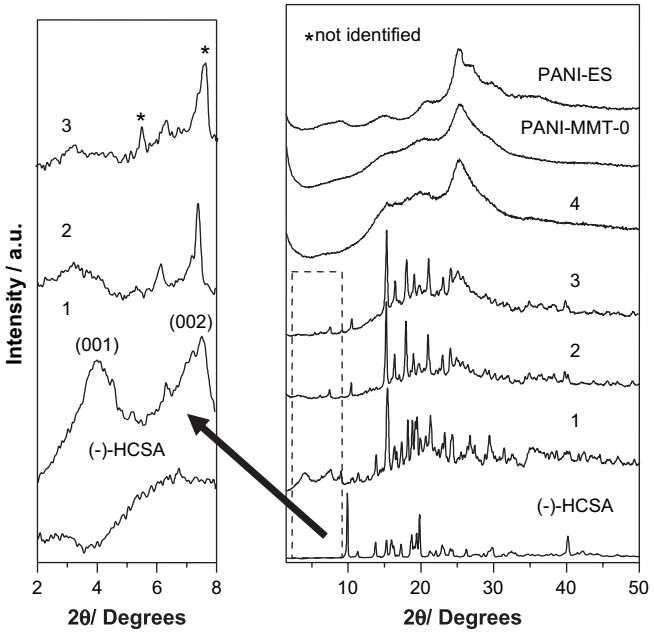

Fig. 2. XRD patterns of powdered samples of PANI–MMT composites: 1, 2, 3, 4. XRD patterns of (−)HCSA, PANI–MMT-0 and PANI-ES samples are also shown for comparison purposes.

for example, with HSCA through hydrogen bonding and facilitating the organic molecule crystallization.

X-ray diffraction pattern of PANI–MMT-1 shows low intensity and broad peaks at low angle ($2\theta < 8°$) while a halo ($2\theta \sim 25°$) characteristic of PANI type I [14] is observed for PANI–MMT-4. The presence of Bragg diffraction peaks at about 4–4.5° (ca. 22 Å) and 7–8° (ca. 12 Å) for composite-1 (Fig. 2(1)) can be due to clay tactoids having PANI intercalated between the layers. The d_{001} basal spacing is about 21.6 Å and, considering the clay thickness of 9.6 Å, the gallery height is about 12 Å. The (002) reflection can be at $2\theta \sim 7.5°$, where a very broad and asymmetric diffraction peak is observed, probably due to the high disorder in the clay layers stacking. The increase observed in the basal spacing of Na^+–MMT ($d_{001} = 12.8$ Å) suggests that PANI–MMT-1 is an intercalated nanocomposite (nevertheless PANI chains should also be outside clay galleries). The d_{001} value is higher than that observed for PANI–MMT (14.2 Å, Ref. [8b]) obtained by An^+–MMT polymerization. Probably there is more than one polymer chain intercalated between the PANI–MMT-1 layers. Similar values of basal spacing (ca. 16 Å) were reported by Kim et al. [7a,b] for similar PANI–MMT materials.

PANI–MMT composites 2–4 have no peaks that can be attributed to (001) clay tactoids reflection (Fig. 2(2–4)). It is

Table 2
XRD data of PANI–MMT composites and (−)HCSA

Composite-1		Composite 2		Composite 3		HCSA	
2θ/(°)	d/Å	2θ/(°)	d/Å	2θ/(°)	d/Å	2θ/(°)	d/Å
9.05	9.77	9.10	9.72			9.05	9.77
						10.0	8.84
11.4	7.76					11.4	7.76
13.9	6.37					13.9	6.37
15.4	5.75	15.3	5.79	15.4	5.75	15.4	5.75
						16.2	5.47
16.4	5.40	16.5	5.37	16.5	5.37	16.4	5.40
17.4	5.10					17.4	5.10
18.8	4.72					18.8	4.72
19.5	4.55					19.5	4.55
19.9	4.46	19.8	4.48	19.9	4.46	19.9	4.46
21.3	4.17					21.4	4.15
		22.2	4.00			22.1	4.02
		23.1	3.85	23.2	3.83	23.1	3.85
		24.1	3.69	24.2	3.68	24.1	3.69
24.3	3.66	3.66				24.4	3.65
		30.2	2.96			30.0	2.98
40.4	2.23					40.3	2.24

Composite 4 has diffraction peaks at $2\theta = 15.4°$ and 19.9°.

possible to suggest that clay layers are separated and chaotically dispersed throughout the polymer phase forming *exfoliated nanocomposites*. However, conclusions about the composite structure based solely on XRD data are not confident since the absence of (001) reflection can be due a low organization in the layers stacking (causing the peak broadening) and/or a low clay amount in the sample.

PANI–MMT-4 has the lowest amount of clay and an XRD pattern equal to PANI–MMT-0. Fig. 2 also shows XRD pattern of PANI-ES prepared following Ref. [10] which can be characterized as ES-I type structure [14]: $d_{001} = 9.2$ Å (intrachain reflection), $d_{010} = 6$ Å (interchain reflection), $d_{100} = 4.28$ Å (interchain reflection), $d_{110} = 3.56$ Å. According to XRD data, PANI chains arrangement in the solid state is not coincident when doped with HCl (PANI-ES) or with HCSA.

X-ray near edge absorption of Si *K*-edge (Si *K* XANES) technique can be used for monitoring distortions of $[SiO_4]^{4-}$ tetrahedral units [12]. Fig. 3 shows Si *K* XANES spectra of Na^+–MMT, and PANI–MMT composites. The same spectral profiles for all samples are observed. Nevertheless, the first absorption peak shifts as clay content decreases in the composites: 1846.8 eV for PANI–MMT-1, 1846.9 eV for PANI–MMT-2, 1847.0 eV for PANI–MMT-3 and 1847.1 eV for PANI–MMT-4 (Fig. 3(1–4)). Peaks shifting can be associated to distortions in silicon clay sheet [12]. In diluted clay suspensions, there is a high degree of exfoliated particles, i.e. reduction of number of stacked clay layers in *c*-crystallographic direction, producing a colloidal dispersion. This effect turns clay particles more susceptible to ended sheet tension (that could occur in all exfoliated layered materials), leading to certain torsion of clay particles. Thus, Si *K*-edge XANES data corroborate XRD data, suggesting high disorder in the clay layers stacking and high dispersion of clay layers through the polymeric matrix when MMT amount in the composite decreases. In Scheme 1 it is presented a tentative representation

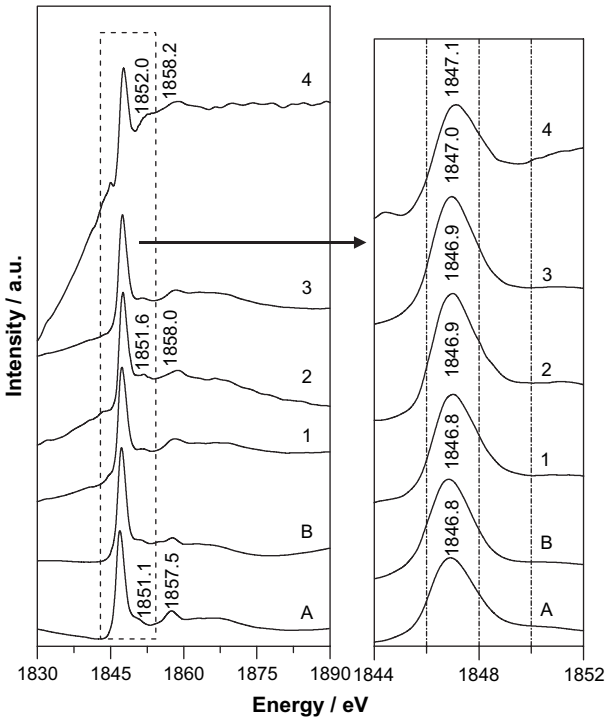

Fig. 3. Silicon *K*-edge XANES spectra of powdered samples of: Na^+–MMT (A); PANI–MMT (from An^+–MMT polymerization) (B), and PANI–MMT composites: 1, 2, 3, 4.

of the structure of PANI–MMT composites, considering SEM, XRD, and Si *K* XANES data.

The UV–VIS–NIR spectra of PANI–MMT samples together with poly(aniline) in its emeraldine salt and base forms (PANI-ES and PANI-EB, respectively) are presented in Fig. 4. PANI-EB is a semiconductor material, but gives the conducting emeraldine salt form after protonation. All these forms

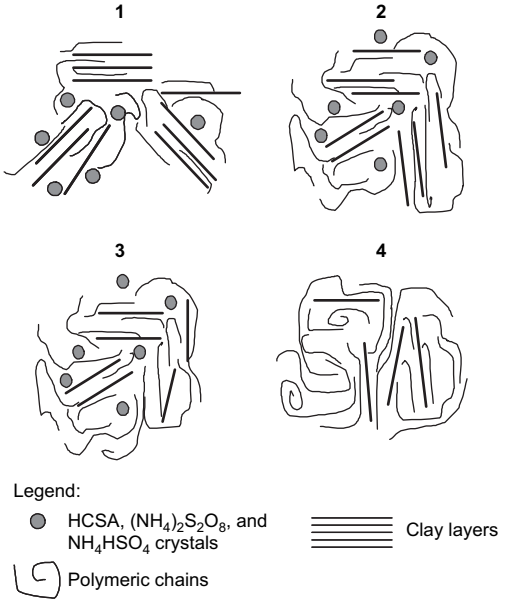

Scheme 1. Schematic representation of possible domains of PANI–MMT composites based on SEM, XRD, and Silicon *K*-edge XANES data.

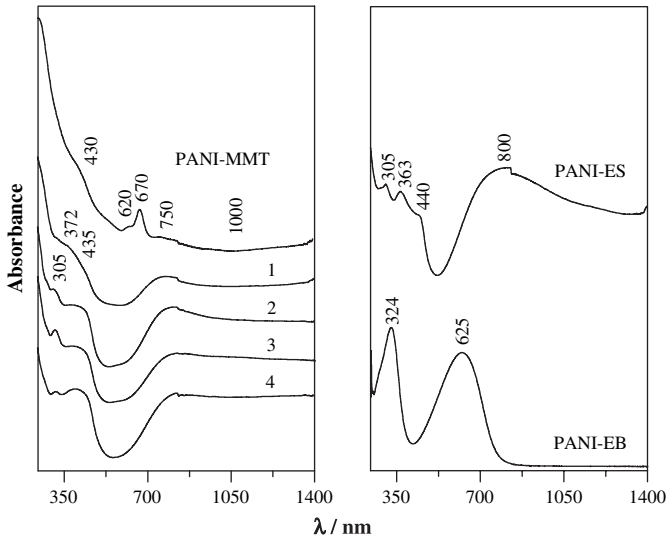

Fig. 4. UV–VIS–NIR spectra of aqueous suspensions of PANI–MMT composites: 1, 2, 3, 4; PANI–MMT (from An^+–MMT polymerization); PANI-EB dissolved in *N*-methyl-pyrrolidone, and PANI-ES dissolved in concentrated HCl.

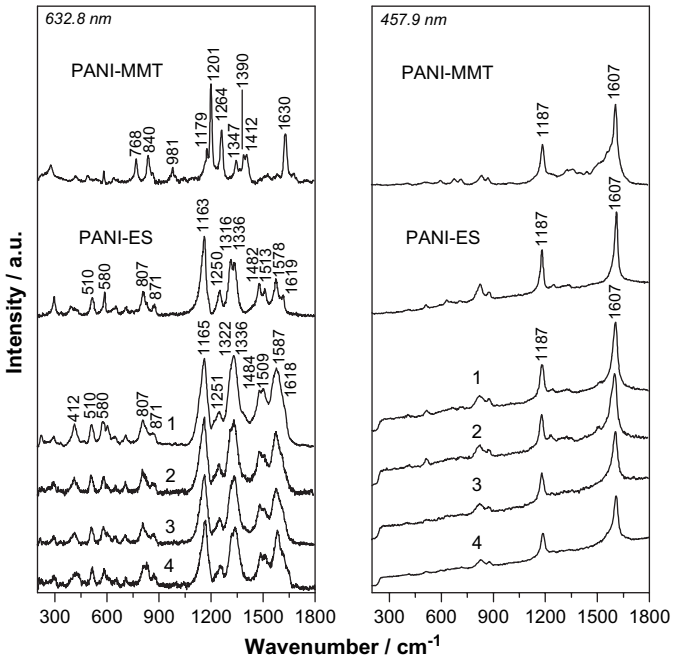

Fig. 5. Resonance Raman spectra for two excitation lines of powdered samples of PANI–MMT composites: 1, 2, 3, 4; PANI-ES, and PANI–MMT (from An^+–MMT polymerization).

have characteristic electronic bands, for which assignments are well known [15a]. For PANI-EB the band at 330 nm corresponds to $\pi \rightarrow \pi^*$ transition and the band at 640 nm has been assigned to the electron transition from benzenoid to quinoid rings [15b]. For PANI-ES the peak at ca. 440 nm and the broad band starting at ca. 600 nm are assigned to electronic absorptions of radical cation segments [8b]. From Fig. 4 it is possible to see that the spectra of PANI–MMT-1, 2, 3, and 4 are very similar to PANI-ES spectrum.

The absorption bands at 620 and 670 nm in PANI–MMT nanocomposite (from An^+–MMT polymerization) spectrum are not observed in any spectra of PANI–MMT composites prepared as described in this work. In a previous work [8b], these bands were assigned to localized transitions in phenazine and azo moieties of the intercalated polymeric chain. The absence of these moieties in composites prepared as described here is a strong evidence that formation of these segments is a direct consequence of confinement of anilinium monomer in MMT.

The resonance Raman spectroscopy technique is sensitive to the electronic structure and the vibrational properties of PANI. Through resonance Raman effect is possible to select different chromophores (radical cations, dications, and benzenoid units) of PANI by changing the excitation radiation [16]. Fig. 5 shows resonance Raman spectra of PANI–MMT samples and PANI-ES at 632.8 nm exciting wavelength. Using this laser line, vibrational bands of radical cations and dications present high relative intensities [16]. Spectra of PANI–MMT composites have the same PANI-ES spectral profile. Bands at 1163, 1619 and duplet at 1316/1336 cm^{-1} are assigned to βC–H, νC–C and νC–N modes of radical cations segments, respectively [16]. Band at 1250 cm^{-1} is assigned to νC–N mode of benzenoid rings (reduced segments) while bands at ca. 1482 and 1578 cm^{-1} are attributed to νC–N and νC–C modes of quinoid rings of dication segments, that are presented in the polymeric chains of PANI-ES. The characteristic bands of phenazinic rings (1201, 1412 and 1630 cm^{-1}) and dication benzidine units (1390 cm^{-1}) are only observed for PANI-MMT nanocomposite prepared from An^+–MMT polymerization (see Fig. 5) [8a,b].

Raman spectra recorded using laser line at 457.9 nm also corroborate the Raman data obtained at 632.8 nm exciting radiation. Using this excitation radiation, benzenoid moieties of PANI-ES are in resonance [16], and bands at 1187 and 1607 cm^{-1}, assigned to βC–H, and νC–C of benzenoid units, respectively are observed in PANI-ES spectrum [16]. The same bands are observed for all PANI–MMT composites. One important point is the non-observation of other bands in those PANI–MMT composite spectra that could be assigned to other chromophores present in polymeric chains. New bands have been observed in the spectrum of PANI–MMT prepared from An^+–MMT polymerization excited at 457.9 nm [8b]. Hence, resonance Raman result is in agreement with electronic absorption data in relation to the nature of the polymeric chains (i.e., PANI–MMT-1, 2, 3 and 4 composites are PANI-ES-like materials).

Fig. 6 shows Nitrogen *K*-edge XANES spectra of PANI–MMT composites and PANI-ES. In the PANI-ES spectrum, the peaks at 399.1 and 402.3 eV can be assigned to radical cation and amine nitrogen, respectively [8b]. The peak at 400.4 eV in the spectra of PANI–MMT composites has been observed in PANI-EB spectrum and was assigned to imines nitrogen from quinone moieties [8b,c]. For PANI–MMT-1 the high relative intensity of the peak at 400.4 eV could be explained considering that for this composite there are more intercalated PANI-ES, where delocalized quinone moieties

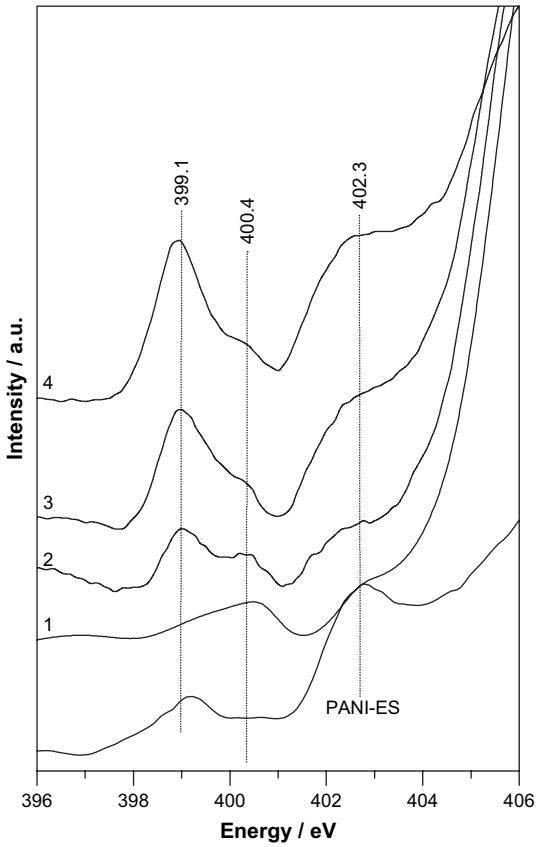

Fig. 6. Nitrogen *K*-edge XANES spectra of solid samples of PANI–MMT composites: 1, 2, 3, 4 and PANI-ES.

become more stable. The increase in the relative intensity of the peak assigned to radical units (at 399.1 eV) with the decrease in the clay amount (see from spectra 2 to 4) can be due to the formation of more polymeric chains outside interlayer cavity.

EPR spectra of PANI–MMT composites shown in Fig. 7 indicate the presence of radical cation in all samples. There is a pronounced decrease of the signal with the increase in the clay amount. This result is in agreement with Nitrogen *K*-edge XANES data.

X-ray photoelectron spectroscopy has been largely used for characterizing PANI nitrogen oxidation states [17]. Fig. 8(A,B) shows characteristic Nitrogen 1s XPS spectra of PANI-EB and PANI-ES. The lines at 398.1 and 399.3 eV in PANI-EB spectrum can be assigned to imine (=N–) and amine (–NH–), respectively, while the low intensity band at 400.8 eV is related to radical ($-\overset{+\bullet}{N}=$) and/or protonated amine ($-\overset{+}{N}H_2-$) nitrogens from non-deprotonated sites in PANI-EB. The lines at 399.2 and 401.3 eV in PANI-ES spectrum are due to amine and radical nitrogens and/or protonated amine, respectively [17]. Spectrum of PANI–MMT-4 (Fig. 8C) presents lines at 399.5, 401.2 and 402.9 eV that can be assigned to amine, radical and/or protonated amine and protonated imine ($-\overset{+}{N}H=$) nitrogens, respectively. The Nitrogen 1s XPS spectrum for PANI–MMT nanocomposite obtained from An^{+}–MMT polymerization (Fig. 8D) was discussed in a previous work [8b].

It is known that XPS signal is extremely sensitive to material surfaces, thus the majority of information comes from the

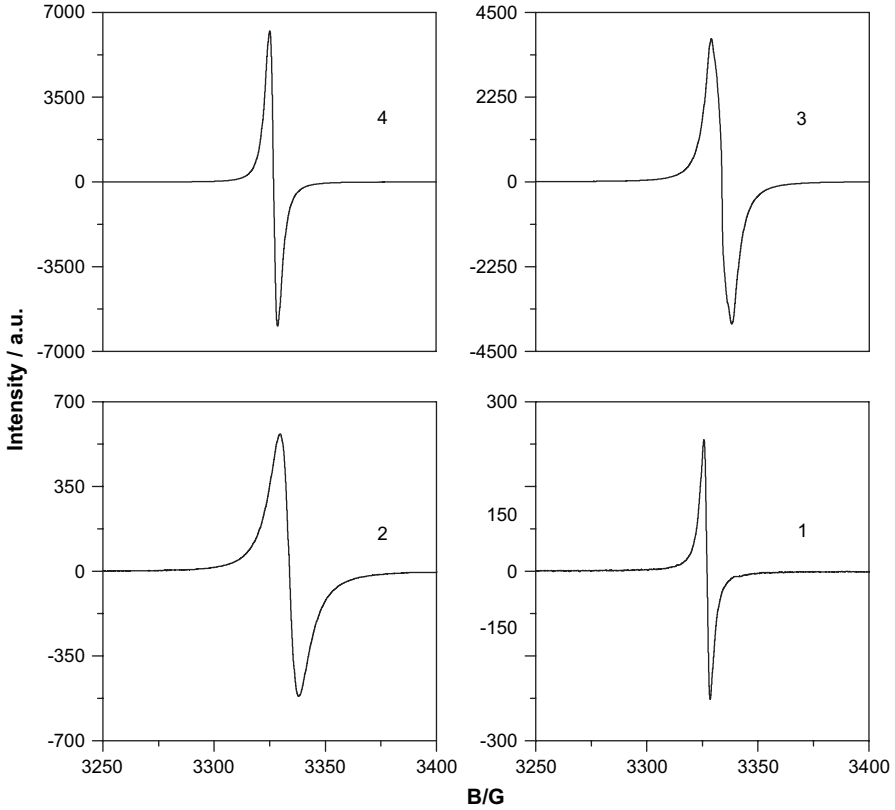

Fig. 7. EPR of solid samples of PANI–MMT composites: 1, 2, 3, 4.

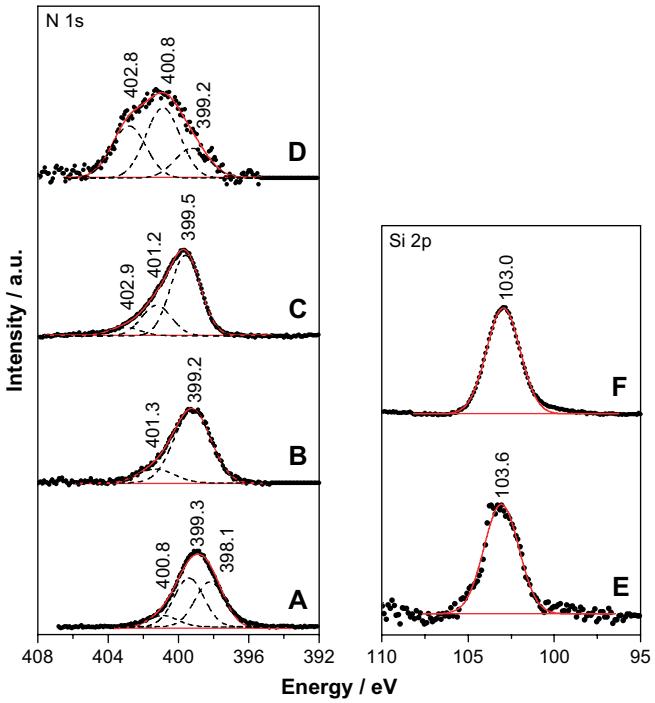

Fig. 8. Nitrogen 1s XPS spectra of solid samples of: PANI-EB (A), PANI-ES (B), PANI–MMT-4 (C), and PANI–MMT (from An^+–MMT polymerization) (D) and Silicon 2p XPS spectra of solid samples of: PANI–MMT-4 (E) and PANI–MMT (from An^+–MMT polymerization) (F).

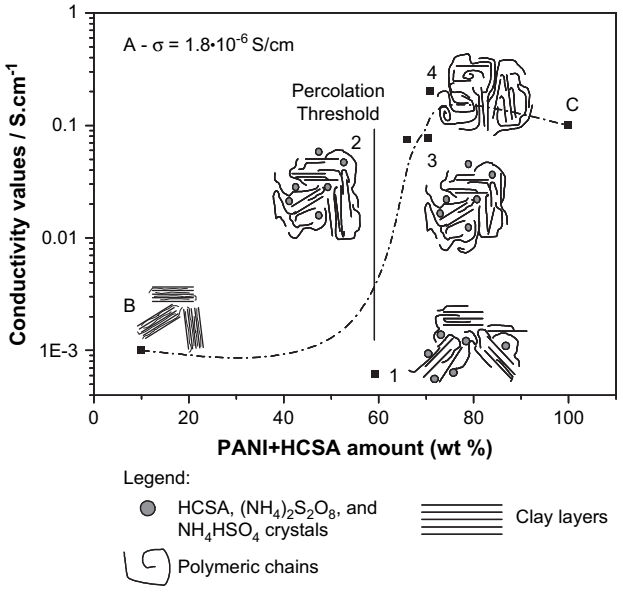

Fig. 9. Conductivity values observed for: Na^+–MMT (A), PANI–MMT (from An^+–MMT polymerization) (B), and PANI–MMT composites: 1, 2, 3, 4, and PANI-ES (C).

first three atomic monolayers of the particle, which means that only polymeric chains on the external surfaces or on the edge of clay crystal contribute to XPS in region of Nitrogen 1s signal of PANI–MMT material. Therefore, low value of N/Si ratio (0.026, see N and Si peaks in Fig. 8D and F, respectively) obtained for PANI–MMT nanocomposite obtained from An^+–MMT polymerization suggests that only a small fraction of polymer is on external clay surface, which is in agreement with SEM images (see Fig. 2B). On the other hand, PANI–MMT-4 exhibits high N/Si ratio (7.78, see N and Si peaks in Fig. 8C and E, respectively) due to a great quantity of polymeric chains located the in external surface of clay particles, which corroborates the SEM images (Figs. 2–4).

Absence of peaks in XPS spectrum of PANI–MMT-4 which can be assigned to nitrogen atoms of phenazinic-like rings and azo units, confirms that these segments are not present in polymeric chains of PANI–MMT composite. This observation reinforces that the nature of polymeric chains on clay surface is similar to that of free PANI chains.

The a.c. conductivity data obtained for PANI–MMT nanocomposites are presented in Fig. 9. It is possible to notice that electrical conductivity of PANI–MMT composites decreases when insulate clay content is increased. An abrupt reduction of conductivity, characteristic to percolation threshold, was observed for composites with less than 60% of organic molecules (PANI and HCSA). Above this mass ratio, conductivity values of PANI–MMT materials with minor clay content (high PANI–MMT mass ratio) have the same free PANI-ES (1×10^{-1} S cm^{-1}) magnitude.

This behavior can be rationalized considering that the changes in composite's conductivity is due to alterations in the structure of intra-chain and inter-chain PANI arrangements and this is promoted by changes in clay amount in the composites. For composites with high clay amount (PANI–MMT-1), the inter-chain connections are broken and conducting polymeric islands are isolated one from the other. Nevertheless, when the clay amount is reduced and dispersion of clay layers is increased in the composites (see Scheme 1, from PANI–MMT-2 to 4), an increase in the composite's conductivity is observed, due to the "re-connection" of conducting polymeric islands. On the other hand, the clay layers can be also changing the intra-chain PANI arrangements and, as a consequence, affecting the delocalization and nature of charge carriers in PANI chains. It is interesting to notice that composite with high clay amount (PANI–MMT-1) has lesser radical cations than the other composites (according XANES and EPR data). Radical cations prevail only when the clay amount in the composites is lesser than about 17%. Probably, when PANI–MMT composites have high level of intercalated PANI chains, the radical cations are not so stable. Hence, this difference in intra-chain PANI arrangements with the change of composite clay amount can also be affecting the values of "bulk" conductivity. It is difficult to know, through "bulk" conductivity values, if the intra-chain PANI arrangements in intercalated nanocomposites are better for electronic delocalization than in exfoliated nanocomposites, because the interchain connections are also affected by polymer intercalation.

4. Conclusion

SEM data show that morphology of PANI–MMT composites changes according to clay amounts. The presence of crystalline phases in PANI–MMT-1, 2, 3 was attributed to the

formation of HCSA, NH_4HSO_4, and $(NH_4)_2S_2O_8$ during the aniline polymerization. Si *K*-edge XANES technique shows that silicate clay sheet suffers distortions in PANI–MMT-4. Through XRD and Si *K*-edge XANES data it is also possible to suggest that the clay layers are chaotically dispersed in PANI–MMT-4.

PANI emeraldine salt form in the four composites was confirmed by all spectroscopic measurements, showing that PANI electronic conduction is via radical cation carriers. However, through N *K*-edge XANES and EPR data it is possible to observe that the increase in clay content in composites leads to a reduction of radical cation segments in PANI chains due to the confinement of the polymeric chains.

Conductivity values of PANI–MMT composites change from 10^{-1} to 10^{-4} S cm^{-1} when the polymer/clay mass ratio was decreased, confirming the presence of a percolation threshold.

Acknowledgments

This work was supported by FAPESP (Brazilian agency). Fellowships from FAPESP (G.M. do Nascimento) and CNPq (M.L.A. Temperini and V.R.L. Constantino) are gratefully acknowledged. The authors would like to thank the National Synchrotron Light Laboratory (LNLS/Brazil) for XANES Nitrogen *K*-edge (SGM 1026, 1427, 1432 and 2169) and Silicon *K*-edge (SXS 1935) measurements and LME/LNLS (LV 2161 and 2166) for technical support during electron microscopy measurements. The authors are also grateful to Dr. A.M.C. Ferreira for the EPR spectra, Dr. S.I.C. de Torresi for conductivity measurements and Dr. P.M. Dias for providing the Na^+–MMT suspension.

References

[1] MacDiarmid AG. Angew Chem Int Ed 2001;40(14):2581–90.
[2] (a) Cardin DJ. Adv Mater 2002;14(8):553–63;
(b) Alexandre M, Dubois P. Mater Sci Eng R 2000;28(1–2):1–63;
(c) Oriakhi CO. J Chem Educ 2000;77(9):1138–46;
(d) Ruiz-Hitzky E, Aranda P. Anales de Quimica Int Ed 1997;93(3):197–212;
(e) Maia DJ, De Paoli MA, Alves OL, Zarbin AJG, Das Neves S. Quim Nova 2000;23(2):204–15.
[3] (a) Han MG, Cho SK, Oh SG, Im SS. Synth Met 2002;126(1):53–60;
(b) Wei Z, Zhang Z, Wan M. Langmuir 2002;18(3):917–21;
(c) Guo X, Luo K, Shi N. J Mater Sci Technol 2005;21(2):179–82.
[4] (a) Huang J, Kaner RB. J Am Chem Soc 2004;126(3):851–5;
(b) Huang J, Kaner RB. Angew Chem Int Ed 2004;43(43):5817–21.
[5] (a) Martin CR. Acc Chem Res 1995;28(2):61–8;
(b) Hulteen JC, Martin CR. J Mater Chem 1997;7(7):1075–87;
(c) Martin CR. Science 1994;266(5193):1961–6.
[6] (a) Wu Q, Xue Z, Qi Z, Hung F. Polymer 2000;41(6):2029–32;
(b) Wu Q, Xue Z, Qi Z, Wang F. Acta Polym Sin 1999;5:551–6;
(c) Chang TC, Ho SY, Chao KJ. J Chin Chem Soc 1992;39(3):209–12;
(d) Feng B, Su Y, Song J, Kong K. J Mater Sci Lett 2001;20(4):293–4;
(e) Inoue H, Yoneyama H. J Electroanal Chem 1987;233(1–2):291–4;
(f) Frisch HL, Xi B, Qin Y, Rafailovich M, Yang NL, Yan X. High Perform Polym 2000;12(4):543–9;
(g) Biswas M, Ray SS. J Appl Polym Sci 2000;77(13):2948–56;
(h) Lee D, Char K, Lee SW, Park YW. J Mater Chem 2003;13:2942–7.
[7] (a) Kim BH, Jung JH, Kim JW, Choi HJ, Joo J. Synth Met 2001;117(1–3):115–8;
(b) Kim BH, Jung JH, Kim JW, Choi HJ, Joo J. Synth Met 2001;121(1–3):1311–2;
(c) Kim BH, Jung JH, Joo J, Kim JW, Choi HJ. J Korean Phys Soc 2000;36(6):366–70.
[8] (a) Do Nascimento GM, Constantino VRL, Temperini MLA. Macromolecules 2002;35(20):7535–7;
(b) Do Nascimento GM, Constantino VRL, Landers R, Temperini MLA. Macromolecules 2004;37(25):9373–85;
(c) Do Nascimento GM, Constantino VRL, Temperini MLA. J Phys Chem B 2004;108(18):5564–71;
(d) Do Nascimento GM, Temperini MLA. Quim Nova 2006;29(4):823–8.
[9] Glingerman ML, King JA, Schulz KH, Meyers JD. J Appl Polym Sci 2002;83(6):1341–56.
[10] MacDiarmid AG, Chiang JC, Richter AF, Sonosiri NLD. Conducting polymers. In: Alcácer L, editor. Dordrecht: Reidel Publications; 1987. p. 105.
[11] Vinogradov AS, Akimov VN. Opt Spectrosc 1998;85(1):53–9.
[12] (a) Li D, Bancroft GM, Fleet ME, Feng XH. Phys Chem Miner 1995;22(2):115–22;
(b) Pong WF, Chang YK, Mayanovic RA, Ho GH, Lin HJ, Ko SH, et al. J Electron Spectrospec Relat Phenom 1996;78:107–10.
[13] (a) JCPD11-0551;
(b) JCPD35-1500.
[14] Pouget JP, Jozefowicz ME, Epstein AJ, Tang X, MacDiarmid AG. Macromolecules 1991;24(3):779–89.
[15] (a) Libert J, Cornil J, Dos Santos DA, Brédas JL. Phys Rev B 1997;56(14):8638–50;
(b) Huang WS, MacDiarmid AG. Polymer 1993;34(9):1833–45.
[16] (a) Furukawa Y, Ueda F, Hyodo Y, Harada I, Nakajima T, Kawagoe T. Macromolecules 1988;21(5):1297–305;
(b) Furukawa Y, Hara T, Hyodo Y, Harada I. Synth Met 1986;16(2):189–98;
(c) Louarn G, Lapkowski M, Quillard S, Pron A, Buisson JP, Lefrant S. J Phys Chem 1996;100(17):6998–7006.
[17] (a) Nakajima T, Harada M, Osawa R, Kawagoe T, Furukawa Y, Harada I. Macromolecules 1989;22(6):2644–8;
(b) Tan KL, Tan BTG, Kang ET, Neoh KG. Phys Rev B 1989;39(11):8070–3;
(c) Monkman AP, Stevens GC, Bloor D. J Phys D Appl Phys 1991;24(5):738–49;
(d) Zeng X-R, Ko T-M. Polymer 1998;39(5):1187–95.